Journal of Quantitative Spectroscopy & Radiative Transfer 160 (2015) 36–49

Contents lists available at ScienceDirect

Journal of Quantitative Spectroscopy & Radiative Transfer

journal homepage: www.elsevier.com/locate/jqsrt

# Retrieval of ethane from ground-based FTIR solar spectra using improved spectroscopy: Recent burden increase above Jungfraujoch

B. Franco [a,*], W. Bader [a], G.C. Toon [b], C. Bray [c], A. Perrin [d], E.V. Fischer [e], K. Sudo [f,g], C.D. Boone [h], B. Bovy [a], B. Lejeune [a], C. Servais [a], E. Mahieu [a]

[a] Institute of Astrophysics and Geophysics, University of Liège, B-4000 Liège (Sart-Tilman), Belgium
[b] Jet Propulsion Laboratory, California Institute of Technology, Pasadena, CA 91109, USA
[c] CEA, DEN, DPC, F-91191 Gif-sur-Yvette, France
[d] Laboratoire Interuniversitaire des Systèmes Atmosphériques (LISA-UMR7583) CNRS, Universités Paris Est Créteil and Paris 7 Diderot (IPSL), F-94010 Créteil cedex, France
[e] Department of Atmospheric Science, Colorado State University, Fort Collins, CO, USA
[f] Graduate School of Environmental Studies, Nagoya University, Nagoya, Japan
[g] Department of Environmental Geochemical Cycle Research, Japan Agency for Marine-Earth Science and Technology, Yokohama, Japan
[h] Department of Chemistry, University of Waterloo, Ontario, Canada

ARTICLE INFO

*Article history:*
Received 11 December 2014
Received in revised form
12 March 2015
Accepted 13 March 2015
Available online 20 March 2015

*Keywords:*
Ethane
FTIR
Jungfraujoch
Pseudo-lines
Trend
Shale gas

ABSTRACT

An improved spectroscopy is used to implement and optimize the retrieval strategy of ethane ($C_2H_6$) from ground-based Fourier Transform Infrared (FTIR) solar spectra recorded at the high-altitude station of Jungfraujoch (Swiss Alps, 46.5°N, 8.0°E, 3580 m a.s.l.). The improved spectroscopic parameters include $C_2H_6$ pseudo-lines in the 2720–3100 $cm^{-1}$ range and updated line parameters for methyl chloride and ozone. These improved spectroscopic parameters allow for substantial reduction of the fitting residuals as well as enhanced information content. They also contribute to limiting oscillations responsible for ungeophysical negative mixing ratio profiles. This strategy has been successfully applied to the Jungfraujoch solar spectra available from 1994 onwards. The resulting time series is compared with $C_2H_6$ total columns simulated by the state-of-the-art chemical transport model GEOS-Chem. Despite very consistent seasonal cycles between both data sets, a negative systematic bias relative to the FTIR observations suggests that $C_2H_6$ emissions are underestimated in the current inventories implemented in GEOS-Chem. Finally, $C_2H_6$ trends are derived from the FTIR time series, revealing a statistically-significant sharp increase of the $C_2H_6$ burden in the remote atmosphere above Jungfraujoch since 2009. Evaluating cause of this change in the $C_2H_6$ burden, which may be related to the recent massive growth of shale gas exploitation in North America, is of primary importance for atmospheric composition and air quality in the Northern Hemisphere.



## 1. Introduction

Ethane ($C_2H_6$) is the most abundant non-methane hydrocarbon in the Earth's atmosphere with a lifetime of approximately 2 months [1]. On a global scale, the main

* Corresponding author. Tel.: +32 4 366 97 85.
*E-mail address:* bruno.franco@ulg.ac.be (B. Franco).

http://dx.doi.org/10.1016/j.jqsrt.2015.03.017
0022-4073/

sources of $C_2H_6$ are leakage from the production, transport of natural gas loss (62%), biofuel consumption (20%) and biomass burning (18%), mainly located in the Northern Hemisphere [1–3]. Biogenic and oceanic sources are generally very small [1]. The main sink of $C_2H_6$ in the troposphere is oxidation via reaction with hydroxyl radicals (OH), while in the stratosphere reaction with chlorine atoms dominates [4].

Ethane has a large impact on tropospheric composition and impacts the distribution of ozone ($O_3$) through several pathways, making it a compound of great interest as a sensitive indicator of tropospheric pollution and transport [5]. By acting as a major sink for tropospheric OH, the abundance of $C_2H_6$ impacts the lifetime of methane ($CH_4$). Thus $C_2H_6$ is an indirect greenhouse gas with a net global warming potential of 5.5 (100-year horizon; [6]). Similarly, $C_2H_6$ influences the atmospheric content of carbon monoxide (CO; [4]). Ethane also has a significant impact on air quality as it is an important source of peroxyacetyl nitrate (PAN), a thermally unstable reservoir for nitrogen oxide radicals ($NO_x$; [1,7]). By providing the main $NO_x$ source in many regions of the atmosphere, PAN has a major effect on the production and loss of $O_3$.

Atmospheric $C_2H_6$ abundances can be measured using various techniques. Previous measurements of $C_2H_6$ include Fourier Transform InfraRed (FTIR) spectrometer observations by the balloon-borne Jet Propulsion Laboratory MkIV Interferometer [8], aircraft air samples collected during the NASA's Global Tropospheric Experiment Field Missions Pacific Exploratory Mission (e.g., PEM-West A; [9] and TRACE-A; [10,11]), solar occultations recorded by the Atmospheric Chemistry Experiment – Fourier Transform Spectrometer (ACE-FTS; [12]), ground-based measurements by gas chromatograph (e.g., [13–15]) and finally limb-scans performed by the Michelson Interferometer for Passive Atmospheric Sounding (MIPAS) onboard the European ENVIronmental SATellite (ENVISAT; [16]). Analysis of these data records has significantly increased our understanding of the long range transport of $C_2H_6$.

Ethane has also been measured by ground-based FTIR technique at several latitudes in both hemispheres, covering different time periods (e.g., [5,17–25]). Nevertheless, strong latitudinal, seasonal and local fluctuations on small spatial and temporal scales make $C_2H_6$ secular trend determination difficult from the existing observations. Indeed, its concentration in the atmosphere is largely influenced by strong vertical mixing and dilution with background air during transport from emission sources.

In this paper, we present a 20-year long-term time series of $C_2H_6$ derived from ground-based high-resolution infrared solar spectra recorded with a Bruker 120HR FTIR spectrometer operated under clear sky conditions at the high-altitude International Scientific Station of the Jungfraujoch (referred to below as ISSJ; Swiss Alps, 46.5°N, 8.0°E, 3580 m a.s.l.; [26]). Such a long-term time series in the remote atmosphere allows for air quality monitoring and provides a valuable tool for model and satellite validation. The solar spectra used here have been recorded within the framework of the Network for Detection of Atmospheric Composition Change monitoring activities (NDACC; see http://www.ndacc.org).

This work furthers the $C_2H_6$ dataset previously published in [19] and [27] for the ISSJ station and it presents an improved retrieval strategy in terms of reduced residuals and enhanced information content, combining three spectral domains for the first time at ISSJ. A careful selection of the available spectroscopic datasets is performed in order to minimize the fitting residuals. A thorough discussion of the retrieval strategy and data characterization (information content and error budget) is presented here along with trend analysis and preliminary comparison with the three-dimensional state-of-the-art global chemical transport model (CTM) GEOS-Chem.

This paper is organized as follows. A detailed description of the optimized retrieval strategy is given in Section 2. Section 3 reports the characterization of the FTIR geophysical products and provides a detailed error budget. Supporting model simulations are described in Section 4. Section 5 presents a preliminary comparison between FTIR and GEOS-Chem seasonal cycles of the $C_2H_6$ burden above Jungfraujoch as well as the entire 1994–2014 time series of daily-mean total columns and corresponding trends. Section 6 concludes this study with a short summary and discussions of the results, identifying avenues for future work.

## 2. FTIR data set

### 2.1. Instrumental setup

All the spectra analyzed here have been recorded at ISSJ, located in the Swiss Alps at 3580 m altitude on the saddle between the Jungfrau (4158 m a.s.l.) and the Mönch (4107 m a.s.l.) summits. This station offers excellent conditions to perform solar observations, particularly in the infrared, because of weak local pollution (no major industries within 20 km) and very high dryness thanks to the high-altitude and the presence of the Aletsch Glacier. Indeed, the amount of water vapor ($H_2O$), a strong interference in the infrared, is at least 20 times lower than at the sea level. Due to these factors, the ISSJ station allows for investigating the atmospheric background conditions over central Europe and the mixing of air masses from planetary boundary layer and free troposphere (e.g., [28,29]).

Here we use observations performed with a commercial Bruker IFS120HR instrument [26]. This spectrometer, affiliated to the NDACC network since 1991, is equipped with HgCdTe and InSb cooled detectors covering the 650–4500 $cm^{-1}$ region of the electromagnetic spectrum.

The Bruker observational database investigated in the present study consists of more than 11,500 spectra recorded between September 1994 and August 2014 with an optical filter covering the 2400–3100 $cm^{-1}$ range encompassing the perpendicular $\nu_7$ fundamental stretching band of $C_2H_6$. Spectral resolutions, defined as the reciprocal of twice the maximum optical path difference, alternate between 0.004 and 0.006 $cm^{-1}$. The signal-to-noise (S/N) ratio varies between 300 and 4500 (average spectra resulting from several successive individual Bruker scans, when solar zenith angles vary slowly). The optimization of

the retrieval strategy has been based on a subset of about 600 spectra during 2003.

### 2.2. Retrieval strategy

The $C_2H_6$ column retrievals and profile inversions have been performed using the SFIT-2 v3.91 fitting algorithm. This retrieval code has been specifically developed to derive mixing ratio profiles of atmospheric species from ground-based FTIR spectra [17]. It is based on the semi-empirical implementation of the Optimal Estimation Method (OEM) developed as in [30]. Vertical profiles are derived from simultaneous fits to one or more spectral intervals of at least one solar spectrum with a multilayer, line-by-line calculation that assumes a Voigt line shape [31].

For the first time at ISSJ, $C_2H_6$ retrievals have been carried out using three micro-windows simultaneously (see Table 1). The first micro-window (MW1) is centered on the well-known strong and sharp $^pQ_3$ sub-branch of the perpendicular $\nu_7$ fundamental stretching band [32] and extends from 2976.660 to 2977.059 $cm^{-1}$. This $^pQ_3$-MW1 is the only one taken into account previously for the Jungfraujoch station [19,27] and at many other FTIR sites (e.g., [21–23,33]). The second micro-window (MW2) includes the $^pQ_1$ sub-branch around 2983.3 $cm^{-1}$, as suggested in [34] and used in [24] in combination with MW1, and extends from 2983.200 to 2983.500 $cm^{-1}$. Finally, a third micro-window (MW3) encompasses the $^rQ_0$ $C_2H_6$ sub-branch around 2986.7 $cm^{-1}$, extending from 2986.450 to 2986.850 $cm^{-1}$. The MW3 has only been fitted at dry high-latitude sites [25,35] because of strong $H_2O$ interferences. Within these micro-windows, the major interfering species whose vertical profiles are scaled during the retrieval process are $CH_4$, $H_2O$, $O_3$ and methyl chloride ($CH_3Cl$).

The model atmosphere adopted above the altitude of the ISSJ station consists of a 39-layer scheme extending from 3.58 km up to 100 km with progressively increasing thicknesses. The pressure–temperature profiles are provided by the National Centers for Environmental Prediction (NCEP, Washington DC, USA, http://www.ncep.noaa.gov/) while the solar line compilation supplied by [36] has been assumed for the non-telluric absorptions.

The $C_2H_6$ a priori mixing ratio profile corresponds to a mean of a 2007–2009 CHASER (Chemical AGCM for Study of atmospheric Environment and Radiative forcing; [37]) simulation (Fig. 1a; see Section 4.1). A priori profiles for all interfering molecules are based on the 1980–2020 simulation of the WACCM model (version 6 of WACCM profiles; the Whole Atmosphere Community Climate Model; e.g., [38]) for the ISSJ station.

In a usual OEM, the covariance matrix should reflect the natural variability of the target gas profile [39]. It is specified for each layer as a percentage of the a priori profile and an ad hoc correlation length, which is interpreted as a correlation between layers decaying along a Gaussian. For $C_2H_6$, we have adopted the relative standard deviation profile derived from the CHASER results (Fig. 1b) as the diagonal values of the covariance matrix and a Gaussian inter-layer correlation with a half-width length of 4 km for extra diagonal elements of the covariance matrix.

It is worth noting that this $C_2H_6$ retrieval strategy has been optimized in such a way to limit the fraction of retrieved profiles presenting negative mixing ratios. By setting up an inter-layer correlation of 4 km and the S/N ratio for inversion at 300, the retrieved information content at Jungfraujoch is slightly constrained deliberately but the retrieval process is stabilized and strong oscillations in the lower levels of the retrieved profiles are avoided. This way, less than 9% of solar spectra have been rejected because of ungeophysical retrieved mixing ratio values. Moreover, statistics have shown that there is no correlation between the seasonality and the fraction of rejected solar spectra. Hence we ensure here homogeneous data coverage and sampling throughout the entire time series (see Section 5.2).

**Table 1**
List of the micro-windows used for the FTIR retrieval of $C_2H_6$ at Jungfraujoch and the interfering species taken into account. Simple scaling of the corresponding vertical profiles of the interfering species is allowed throughout the iterative retrieval process.

| Micro-windows ($cm^{-1}$) | Interfering species |
|---|---|
| 2976.660–2977.059 | $H_2O$, $O_3$, $CH_3Cl$, $CH_4$ |
| 2983.200–2983.500 | $H_2O$, $O_3$, $CH_3Cl$, $CH_4$ |
| 2986.450–2986.850 | $H_2O$, $O_3$, $CH_3Cl$, $CH_4$ |

### 2.3. Spectroscopy

Ethane has a complicated spectrum with 12 interacting normal vibration modes, which makes it difficult to accurately predict the spectrum. Therefore, it is essential to take a closer look at the spectroscopic parameters. First $C_2H_6$ line parameters go back to the work of [40] with the assignment of $C_2H_6$ transitions but no $^pQ$-branches were included. In 1987, to support the Atmospheric Trace Molecule Spectroscopy (ATMOS) Experiment, an empirical linelist for the 9 strongest $^pQ$-branches of $C_2H_6$ covering the 2973–3001 $cm^{-1}$ region was developed [41]. Pacific North West National Laboratory (PNNL, Washington, USA, http://nwir.pnl.gov) measured $C_2H_6$ cross-sections from 700 to 6500 $cm^{-1}$ at a 0.1 $cm^{-1}$ resolution while a quantum mechanically based linelist for the $^pQ_3$ branch at 2976 $cm^{-1}$ was developed [32] and included in the HITRAN 2004 database [42]. The latest HITRAN $C_2H_6$ update (July 2007) contains Pine and Rinsland $^pQ_3$ branch as well as Brown's empirical linelist for the 8 other $^pQ$-branches but still lacks information for weaker absorptions features.

Quantum-mechanical analysis of the $C_2H_6$ spectrum remains very difficult and is still lacking, except for the $^pQ_3$ branch. The current state of $C_2H_6$ parameters in HITRAN 2004 and HITRAN 2008 [43] is rather unsatisfactory in the 3 μm region for all spectral features other than the $^pQ_3$ branch. A new set of $C_2H_6$ cross-sections was therefore developed [44], based on new high resolution IR spectra recorded with and without additional synthetic air at the Rutherford Appleton Laboratory Molecular Spectroscopy Facility (RAL, UK, http://www.stfc.ac.uk/ralspace/)

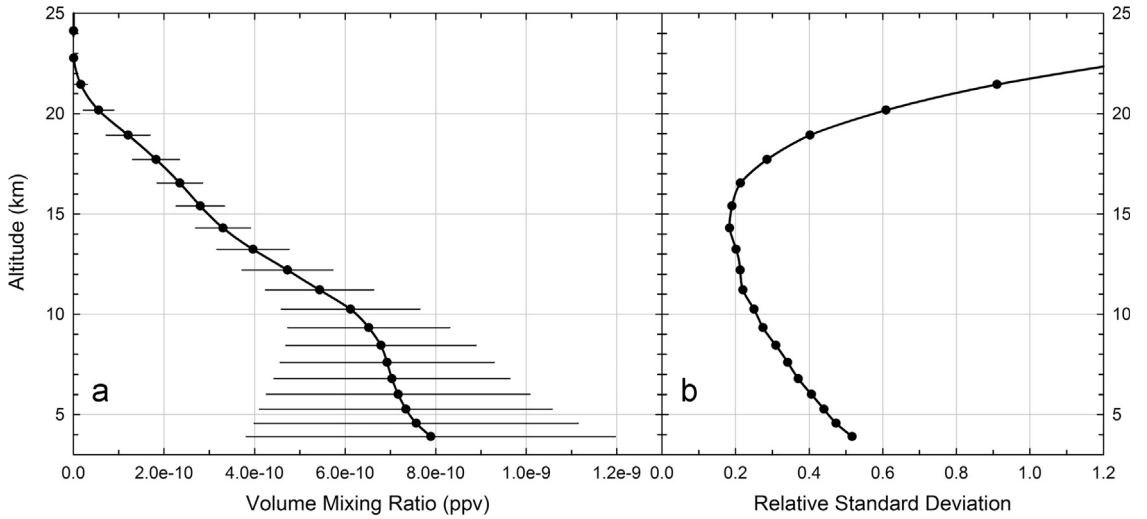


**Fig. 1.** (a) $C_2H_6$ a priori profile with 1-$\sigma$ standard deviation derived from a 2007–2009 CHASER simulation used for the FTIR retrievals at Jungfraujoch. (b) Averaged relative standard deviation of $C_2H_6$ VMR derived from the same CHASER simulation and used as diagonal elements of the covariance matrix for the FTIR retrievals.

using a high resolution FTIR spectrometer. These cross sections for $C_2H_6$ have been measured in the 3 μm spectral region and calibrated in intensity by using low resolution spectra from the PNNL IR database as a reference. Finally, Lattanzi et al. [45] published a linelist including an improved representation of P- and R-branch lines of $C_2H_6$. However, based on the quality of fits to Harrison's lab spectra, it has been evaluated that the Q-branch features which we use for our retrieval strategy are poorly represented compared to HITRAN 2008, (evaluation of this linelist can be found at http://mark4sun.jpl.nasa.gov/report/Evaluation_of_Lattanzi_C2H6_linelist.pdf).

In 2011, an empirical pseudo-line-list (PLL) was fitted to Harrison's $C_2H_6$ lab spectra (the PLL and description can be found at http://mark4sun.jpl.nasa.gov/pseudo.html). The PLL generally provides a convenient and accurate way of interpolating/extrapolating in temperature and pressure to conditions not covered by lab measurements (Harrison's measurements in the case of this study for $C_2H_6$). In the present work, these pseudo-lines have been combined and tested with three versions of HITRAN (i.e. 2004, 2008 and 2012; [42,43,46]).

As the 2950–3020 $cm^{-1}$ region encompasses absorption features from many atmospheric gases, the related spectroscopic parameters need to be as complete and accurate as possible in order to best simulate the atmospheric spectra. To this end, in addition to the $C_2H_6$ PLL, two updates have been included in our linelist. The first one consists of an update for three $O_3$ lines (encompassed in MW1) provided by P. Chelin (Laboratoire de Physique Moléculaire pour l'Atmosphère et l'Astrophysique, Paris, France, Personal Communication, 2004) in the framework of the UFTIR (Time series of Upper Free Troposphere observations from an European ground-based FTIR network) project. The second update concerns the $CH_3Cl$ line positions and line intensities for the $\nu_1$, $\nu_4$ and $3\nu_6$ $CH_3Cl$ bands in the 3.4 μm region (see [47,48]). Fourier transform spectra have been recorded at high resolution at the Laboratoire de Dynamique, Interactions et Réactivité in France. Measurements of line positions and line intensities have been performed for both isotopologues $^{12}CH_3$ $^{35}Cl$ and $^{12}CH_3$ $^{37}Cl$ in the $\nu_1$, $\nu_4$, $3\nu_6$ bands and line intensities have been compared to the recent integrated intensities from PNNL.

Table 2 summarizes the residuals (relative to observations) and mean retrieved columns associated with the use of the HITRAN 2004 (including the August 2006 updates; e.g., [49]), 2008 and 2012 compilations with the different spectroscopic improvements mentioned above. Note that the $CH_3Cl$ update tested here is already part of the original HITRAN 2012 release. These tests have been performed on a subset of 229 representative solar spectra from the year 2003. Fig. 2 displays mean observed and calculated spectra as well as residuals, and illustrates the improvement of residuals brought by each update compared to the initial HITRAN 2008 database. By comparing residuals for each micro-window, we can evaluate the major contributions brought by the $C_2H_6$ PLL and $O_3$ updates (Fig. 2b) compared to the original HITRAN 2008 parameters (Fig. 2a). Finally, Fig. 2c shows a refinement of residuals on the edges of MW1 and MW3 due to the use of the $CH_3Cl$ update. From Table 2 it appears that HITRAN 2008 along with the three updates minimizes the residuals in all micro-windows and hence is currently the best spectroscopic database to employ for ISSJ solar spectra. It is worth noting that the increased residuals observed with the HITRAN 2012 compilation compared to the set up using HITRAN 2008, especially in MW2 (see Table 2), are due to changes in $H_2O$ parameters, more particularly in temperature and pressure-dependency parameters of the $H_2O$ feature at 2983.316 $cm^{-1}$.

## 3. Data characterization and error budget

### 3.1. Characterization of the FTIR retrievals

The averaging kernel matrix (**A**) is resulted by the inversion process of FTIR solar spectra and characterizes

**Table 2**
Root mean square (RMS) residuals of the calculated spectra relative to observations (in %) for each micro-window when fitting a representative subset of 229 solar spectra from the year 2003 and using different combinations of spectroscopic parameters (see first column). These residuals are displayed in Fig. 2 for the HITRAN 2008 compilation and updates. Note that HITRAN 2004 includes the August 2006 updates and that the $CH_3Cl$ update tested here is already part of the original HITRAN 2012 release. The averages of the resulting column values ( $\times 10^{16}$ molec $cm^{-2}$) are listed in the last column. A typical and representative standard deviation of 25% is associated with these mean columns.

| Spectroscopic parameters | RMS (%) | | | Mean column ( $\times 10^{16}$ molec $cm^{-2}$) |
|---|---|---|---|---|
| | MW1 | MW2 | MW3 | |
| HITRAN 2004 | 0.2118 | 0.2974 | 0.5213 | 1.08 |
| HITRAN 2004 + $C_2H_6$ PLL | 0.1905 | 0.2283 | 0.1626 | 1.00 |
| HITRAN 2004 + $C_2H_6$ PLL + $O_3$ | 0.1406 | 0.2283 | 0.1648 | 0.99 |
| HITRAN 2004 + $C_2H_6$ PLL + $O_3$ + $CH_3Cl$ | 0.1158 | 0.2357 | 0.1410 | 1.01 |
| HITRAN 2008 | 0.4705 | 0.1772 | 0.5200 | 1.03 |
| HITRAN 2008 + $C_2H_6$ PLL | 0.1329 | 0.1332 | 0.1627 | 0.97 |
| HITRAN 2008 + $C_2H_6$ PLL + $O_3$ | 0.1316 | 0.1331 | 0.1623 | 0.98 |
| HITRAN 2008 + $C_2H_6$ PLL + $O_3$ + $CH_3Cl$ | 0.1067 | 0.1179 | 0.1379 | 0.99 |
| HITRAN 2012 + $C_2H_6$ PLL + $O_3$ | 0.1230 | 0.2151 | 0.1657 | 0.96 |

the information content of the retrievals. It describes how the retrieved concentration and vertical distribution of an absorber in the atmosphere are related to the true profile ($x_t$) and also provides the contribution of the a priori ($x_a$) to the retrieved profile ($x_r$) according to Eq. (1).

$$x_r = x_a + \mathbf{A}(x_t - x_a) \quad (1)$$

Fig. 3 displays the mean averaging kernels for each vertical layer (Fig. 3b; expressed in molec $cm^{-2}$ / molec $cm^{-2}$) and calculated on the basis of the 2008–2010 individual retrieved profiles, as well as the leading eigenvalues and eigenvectors (Fig. 3a). The vertical sensitivity of our retrieval strategy is illustrated by the total column averaging kernel drawn in black dashed line in Fig. 3b (here with values divided by 10 for visibility purpose). It indicates very good sensitivity to the true state of the atmosphere below ~13 km altitude, with 99% of the information content independent from the a priori profile ($\boldsymbol{x_a}$) and mainly provided by the first eigenvector. The second and third eigenvectors and their associated eigenvalues indicate that the sensitivity of the retrievals extends in the lower stratosphere up to ~20 km, with some additional vertical resolution.

With a mean degree of freedom for signal (DOFS) of $2.11 \pm 0.27$ (1-$\sigma$ confidence interval calculated over all 2008–2010 fitted spectra) and the two leading eigenvalues equal to 0.99 and 0.86, two independent pieces of information may be deduced from the averaging kernels. A first partial column is derived in the lower troposphere (from the ISSJ elevation up to ~8.5 km altitude) and a second one spanning the 8.5–22 km altitude range is identified in the upper troposphere – lower stratosphere. The sensitivity of our retrieval strategy is slightly diminishing for altitudes above ~13 km, but a large part of the information content (at least 60%) is still provided by the measurements at the 22 km level. Although independent partial columns are available from the retrieval process at ISSJ, we will only consider total columns of $C_2H_6$ in this study.

When compared with other recent works using pseudo-lines to retrieve $C_2H_6$ amounts, the content of information obtained from our retrievals is consistent with results from e.g., [25] at Eureka, Canada (80.0°N, 86.4°W, 610 m a.s.l.; DOFS = $2.00 \pm 0.20$) who also employed the three micro-windows, and represents a significant improvement compared to previous works carried out at ISSJ, with typical DOFS of about 1.5 when using the $^pQ_3$ feature alone. The simultaneous use of the three non-contiguous micro-windows allows for a significant gain in retrieved information content compared to three non-simultaneous retrievals which would be subsequently averaged. The DOFS obtained from the individual use of each micro-window is $1.51 \pm 0.24$, $1.86 \pm 0.25$ and $1.70 \pm 0.23$ for MW1, MW2 and MW3, respectively.

### 3.2. Error budget

Table 3 summarizes the major sources of uncertainty that may affect the $C_2H_6$ columns retrieved from the ISSJ solar spectra, as well as estimates of their respective contribution to either systematic or random component of the error budget. The total errors are the square root of the sum of the squares of each of the contributing uncertainty sources. Most of the error contributions (excepting when specified below) have been calculated on the basis of all solar spectra from year 2003 according to the sensitivity tests listed in the last column of Table 3. The $C_2H_6$ retrieval is also characterized at ISSJ by an assumed variability of 29.2% and a daily relative standard deviation (calculated here for the days with at least three observations) equal to 4.0%.

The major contribution to the systematic component of the error budget comes from uncertainties on the $C_2H_6$ spectroscopy. An error of 4% on the line intensity from the original spectra measurements has been reported in [44]. In addition, the uncertainty induced by the conversion of $C_2H_6$ cross-sections into pseudo-lines is estimated at 4% (see [52]), including the random error in the pseudo-line spectroscopic parameters and the systematic error due to an imperfect representation of the physics by the pseudo-lines. We have combined the 4% from [44] in quadrature with the 4% from the conversion into pseudo-lines, giving a conservative uncertainty of 5.6% on the $C_2H_6$ absorption. When assuming this uncertainty during the inversion

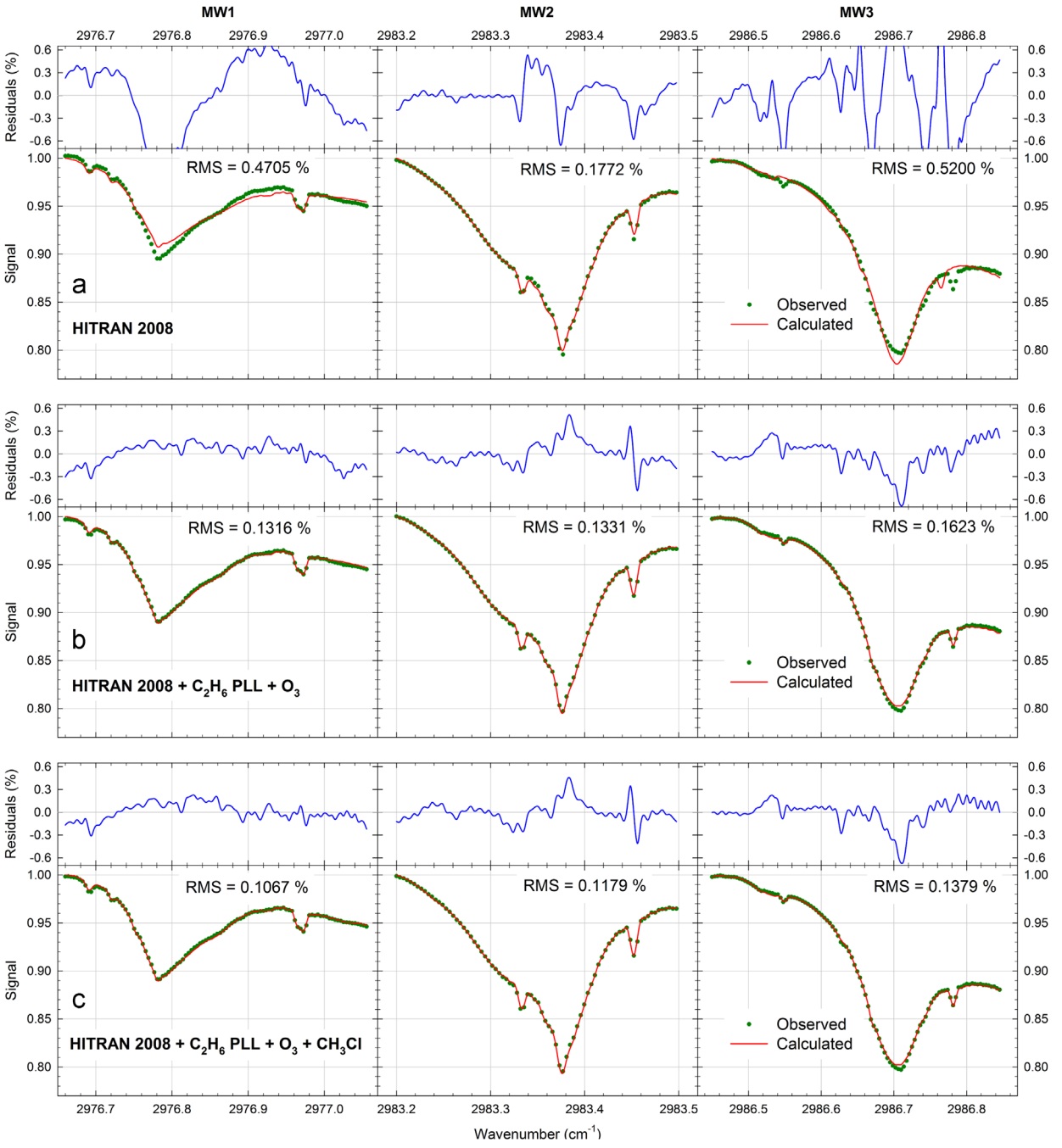


**Fig. 2.** Mean observed (green dots) and calculated (red lines) spectra and associated residuals (obs. – calc.; blue lines) for a representative subset of 229 spectral fits within the three micro-windows used for the $C_2H_6$ retrieval at ISSJ. Spectroscopic compilations used here are (a) the original HITRAN 2008 database, (b) HITRAN 2008 combined with the $C_2H_6$ PLL as well as $O_3$ update and (c) HITRAN 2008 combined with $C_2H_6$, $O_3$ and updated $CH_3Cl$ lines. Note the improvements brought by the different updates on the residuals, whose mean values are also provided in Table 2. (For interpretation of the references to color in this figure caption, the reader is referred to the web version of this paper.)

process, the retrieved $C_2H_6$ columns are affected by systematic anomalies of 5.6%.

Retrieved column biases due to line intensity uncertainties related to the interfering species have been gauged independently by assuming the maximum errors quoted in the HITRAN 2008 (for $H_2O$, $CH_4$ and $O_3$) and HITRAN 2012 (for the $CH_3Cl$ updated line parameters, included in this official release) databases during the fitting process. The column anomalies corresponding to each interfering gas have been combined in quadrature and contribute for 0.9% to the systematic component of the error budget.

Other contributions to the total systematic error are minor. The total columns are retrieved from high quality solar spectra using the SFIT algorithm within uncertainties

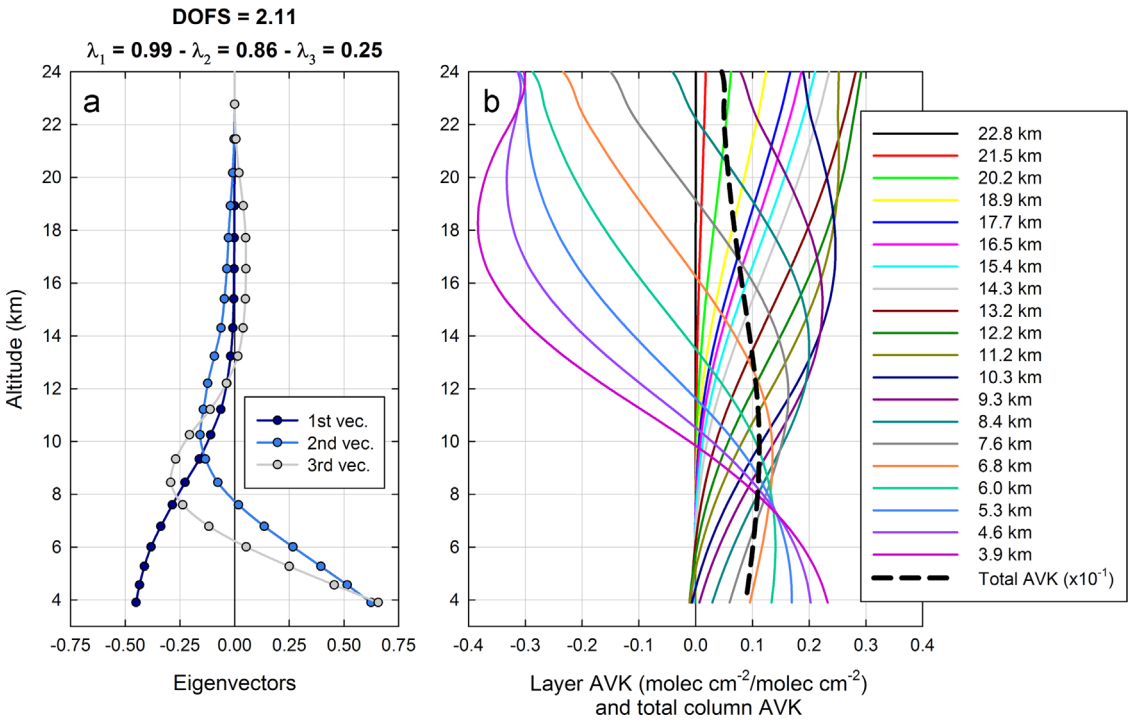


**Fig. 3.** (a) First eigenvectors and associated eigenvalues, and (b) individual averaging kernels for each layer between the 3.6 and 24.0 km altitude range and total column averaging kernel (thick dashed line; divided here by 10 for visibility purpose) characterizing the FTIR retrievals of $C_2H_6$ at ISSJ. The information content has been established on the basis of all the individual retrieved profiles throughout the 2008–2010 time span. The averaging kernels from 2008–2010 are used in Section 5.1 to smooth GEOS-Chem profiles in comparison with the FTIR products. Moreover, tests have shown that the DOFS, eigenvectors and averaging kernels calculated on the basis of other years provide consistent results in terms of information content.

**Table 3**
Error budget of the $C_2H_6$ retrievals at ISSJ, including the impact of systematic and random uncertainties on total columns retrieved from all individual solar spectra recorded during the year 2003, according to specifics given in the last column. The contributions of measurement noise, smoothing and model parameters have been estimated on the basis of a representative subset of solar spectra following the formalism of [50].

| Error source | Error (%) | Comments |
|---|---|---|
| Assumed variability | 29.2 | |
| Relative standard deviation | 4.0 | For the days with at least 3 observations |
| Systematic errors | | |
| $C_2H_6$ spectroscopy and conversion into pseudo-lines | 5.6 | $\pm$5.6% uncertainty on line intensity |
| Line intensity of interfering gases | 0.9 | HITRAN 2008 uncertainties (up to 10% for $H_2O$, 20% for $O_3$, 30% for $CH_4$ and 20% for $CH_3Cl$) |
| ILS | 0.1 | $\pm$10% misalignment and instrument bias |
| Forward model | 1.0 | Retrieval algorithm-related |
| $C_2H_6$ a priori profile | 1.2 | $C_2H_6$ a priori profiles derived from GEOS-Chem and WACCM |
| Total Systematic Error | 5.9 | |
| Random errors | | |
| Temperature profiles | 1.3 | NCEP profile uncertainty (see text) |
| $H_2O$ a priori profile | 0.1 | Changes by a factor of 2 in $H_2O$ a priori slope |
| Solar Zenith Angle (SZA) | 0.8 | $\pm$0.2° bias |
| Measurement noise | 1.6 | |
| Smoothing | 1.1 | |
| Model parameters | 0.2 | |
| Total Random Error | 2.4 | |

estimated at $\pm$1% (see [53]). The impact of an assumed instrumental misalignment of $\pm$10% at the maximum path difference on the retrieved columns is almost negligible (0.1%). Finally, the impact of the selection of the a priori $C_2H_6$ state on the retrieved columns is estimated by adopting other realistic $C_2H_6$ mixing ratio profiles simulated by the GEOS-Chem and WACCM models as a priori, which leads to small divergences by up to 1.2%.

As random errors, we have assumed a 0.2° error in the solar pointing and have adopted the temperature-profile uncertainties quoted by NCEP ($\pm 1.5$ °C between the ground and 20 km altitude, $\pm 2.0$ °C for the 20–30 km altitude range, and from $\pm 5$ °C at 35 km up to $\pm 9$ °C at the stratopause). The corresponding biases on the retrieved $C_2H_6$ columns amount to 0.8 and 1.3%, respectively. As in [54], we have also made the tropospheric slope of the $H_2O$ a priori profile vary by a factor of 2; such perturbations only induce 0.1% bias in the $C_2H_6$ columns, highlighting the independence of the $C_2H_6$ retrieval to the tropospheric water vapor content for a dry high-altitude site.

According to the formalism of [50] and such as detailed in Section 2.2.2 in [51], we have computed the gain and sensitivity matrices of a subset of solar spectra representative of the ISSJ dataset in terms of S/N ratio, DOFS, solar zenith angle, residuals, etc., eventually providing the respective contributions of measurement noise (1.6%), smoothing (1.1%) and forward model parameters (0.2%) to the total random error.

The estimated total systematic and random errors affecting our retrieved $C_2H_6$ columns amount to 5.9 and 2.4%, respectively. The latter represents a significant improvement compared to [19], where only the 2976–2977 $cm^{-1}$ micro-window with the $^pQ_3$ branch for inversion of the ISSJ solar spectra is used and where the random component of the error budget is estimated in a similar way at 6.6% (and also found 5.9% of total bias for the systematic component).

## 4. Supporting model simulations

### 4.1. CHASER

The CHASER model [37,55], developed mainly in the Nagoya University and the Japan Agency for Marine-Earth Science and Technology (JAMSTEC), is a chemistry coupled climate model, simulating atmospheric chemistry and aerosols in cooperation with the aerosol component model SPRINTARS (Spectral Radiation-Transport Model for Aerosol Species; [56]). It has also been developed in the framework of the Model for Interdisciplinary Research on Climate-Earth System Model, MIROC-ESM-CHEM [57]. CHASER simulates detailed chemistry in the troposphere and stratosphere with an on-line aerosol simulation including production of particulate nitrate and secondary organic aerosols.

For this study, the model's horizontal resolution is selected to be $2.8° \times 2.8°$ with 36 vertical layers extending from the surface up to about 50 km altitude. As the overall model structure, CHASER is fully coupled with the climate model core MIROC, permitting atmospheric constituents (both gases and aerosols) to interact radiatively and hydrologically with meteorological fields in the model. For replicating the past meteorological conditions in the model, this study employs a nudged chemical transport model version of CHASER in which wind fields and temperatures calculated by the MIROC's AGCM are relaxed to meteorological reanalysis data. In this study, the NCEP final reanalysis data set is used as a nudging constraint with the HadISST data set (Hadley Centre Sea Ice and Sea Surface Temperature) for distributions of sea surface temperatures and sea ice. Chemistry component of CHASER considers the chemical cycle of $O_x$–$NO_x$–$HO_x$–$CH_4$–CO with oxidation of Non-Methane Volatile Organic Compounds (NMVOCs), halogen chemistry and $NH_x$–$SO_x$–$NO_3$ system simulating 96 chemical species with 287 chemical reactions. In the model, NMVOCs include $C_2H_6$, $C_2H_4$, propane ($C_3H_8$), $C_3H_6$, $C_4H_{10}$, acetone, methanol and biogenic NMVOCs (isoprene, terpenes).

Anthropogenic emissions (for $NO_x$, CO, $CH_4$, NMVOCs, $NH_3$, $SO_2$, black carbon and organic carbon) are specified using the EDGAR-HTAP2 (Emission Database for Global Atmospheric Research, targeted for 2008: http://edgar.jrc.ec.europa.eu/) and fire emissions are based on the MACC's reanalysis data (Monitoring Atmospheric Composition & Change; https://gmes-atmosphere.eu/about/project_structure/input_data/d_fire/) for individual years/months. For biogenic NMVOC emissions, we employ calculation by the land ecosystem/trace gas emission model VISIT (Vegetation Integrative SImulator for Trace gases; [58]).

### 4.2. GEOS-Chem

GEOS-Chem (version 9-01-03: http://acmg.seas.harvard.edu/geos/doc/archive/man.v9-01-03/index.html) is a global 3-D CTM capable of simulating global trace gas and aerosol distributions. GEOS-Chem is driven by assimilated meteorological fields from the Goddard Earth Observing System version 5 (GEOS-5) of the NASA Global Modeling Assimilation Office (GMAO). The GEOS-5 meteorology data have a temporal frequency of 6 h (3 h for mixing depths and surface properties) and are at a native horizontal resolution of $0.5° \times 0.667°$ with 72 hybrid pressure-$\sigma$ levels describing the atmosphere from the surface up to 0.01 hPa. In the framework of this study, the GEOS-5 fields are degraded for model input to a $2° \times 2.5°$ horizontal resolution and 47 vertical levels by collapsing levels above ~80 hPa. The chemical mechanism applied here is the standard full chemistry GEOS-Chem simulation, including detailed $O_3$–$NO_x$–Volatile Organic Compound (VOC) – aerosol coupled chemistry (see [59,60] for full description) with updates by [61].

Ethane is emitted from anthropogenic and pyrogenic sources in GEOS-Chem. The RETRO (REanalysis of the TROpospheric chemical composition) emission inventory [62] is the global default for anthropogenic NMVOC emissions aside from $C_2H_6$ and $C_3H_8$. Ethane and $C_3H_8$ emissions in RETRO are low compared to the GEOS-Chem inventories from [3], which are unbiased relative to the pre-2004 observations presented as in [3]. Thus we used the $C_2H_6$ and $C_3H_8$ emission inventories from [3]. Ethane emissions from biomass burning are from the Global Fire Emissions Database (GFED3) monthly biomass burning emissions [63].

The GEOS-Chem model output presented here covers the period July 2005–May 2013, for which the GEOS-5 meteorological fields are available. We have used a one-year run for spin-up from July 2004 to June 2005, restarted several times for chemical initialization. The model outputs consist of $C_2H_6$ mixing ratio profiles at a 3-h time

frequency, saved at the closest $2^\circ \times 2.5^\circ$ pixel of the ISSJ station. To account for the vertical resolution and sensitivity of the FTIR retrievals, the individual concentration profiles simulated by GEOS-Chem are interpolated onto the vertical grid of FTIR. They are then averaged into daily profiles and eventually smoothed by applying the FTIR averaging kernels **A** (see Eq. (1)) according to the formalism of [39]. The averaging kernels used to convolve the model outputs are seasonal averages over March–May, June–August, September–November and December–February obtained from the 2008–2010 individual FTIR retrievals. The following comparison between FTIR and smoothed GEOS-Chem data involves the days with observations available within the July 2005–May 2013 time period only (i.e. 915 days of observations).

## 5. Ethane time series

In this section, we first present a preliminary comparison between $C_2H_6$ FTIR total columns and simulations by the GEOS-Chem model by illustrating the seasonal cycle of $C_2H_6$ at ISSJ. We have taken into account the vertical resolution and specific sensitivity of the FTIR retrievals before comparison with the model data. We then report the entire 1994–2014 time series of daily-mean total columns and corresponding trends.

### 5.1. Seasonal cycle

The seasonal cycle of $C_2H_6$ abundances above ISSJ is illustrated in Fig. 4, which displays on a 1-year time base the monthly means of FTIR total columns and associated 1-$\sigma$ standard deviation as error bars. The running mean of the FTIR daily average data (not shown here), computed using a 2-month integration length and a 15-day time step, is drawn in solid blue line. The shaded area corresponds to the 1-$\sigma$ standard deviation around the running mean. The FTIR data subset used in Fig. 4 spans the July 2005–May 2013 time period in order to coincide with the GEOS-Chem simulation. A similar running mean and standard deviation have also been calculated on the basis of the daily-averaged total columns simulated by GEOS-Chem (after smoothing by the FTIR averaging kernels). These are represented by the red curve and by the shaded area in Fig. 4, respectively.

The seasonal cycle of $C_2H_6$ apparent in the FTIR total column data and model output are in good agreement, characterized by a maximum in March–April and a minimum in August–September. Since fossil fuel production is the main source of $C_2H_6$ emissions [3] and does not present a particular seasonal cycle during the year [64], the strong seasonal cycle of $C_2H_6$ burden is primarily driven by the photochemical oxidation rate by OH radicals, which is enhanced during summer [65,66]. At mid and high latitudes, $C_2H_6$ accumulates during wintertime and peaks in late winter due to its relatively long lifetime and slow exchange with lower latitudes [19]. Consistent values of seasonal amplitude, i.e. the difference between the maximum and minimum running means divided by the annual average over the whole time period, are associated with these seasonal modulations: 50.4% and 57.3% for FTIR and GEOS-Chem, respectively. A direct comparison between the daily-mean $C_2H_6$ total columns derived from the CTM and ground-based observations is presented in Fig. 5 and shows a correlation $R$ of 0.77.

However, it appears clearly on Figs. 4 and 5 that the $C_2H_6$ burden simulated by GEOS-Chem is systematically lower than the FTIR measurements. Over the mid-2005–mid-2013 time period, the daily-averaged modeled $C_2H_6$ columns present a systematic bias of $-26.7 \pm 16.5\%$ relative to the FTIR daily means, and the two data sets cannot be reconciled by accounting for the systematic errors affecting the observations (see Table 3). The systematic bias is hypothesized to be driven by an underestimation of

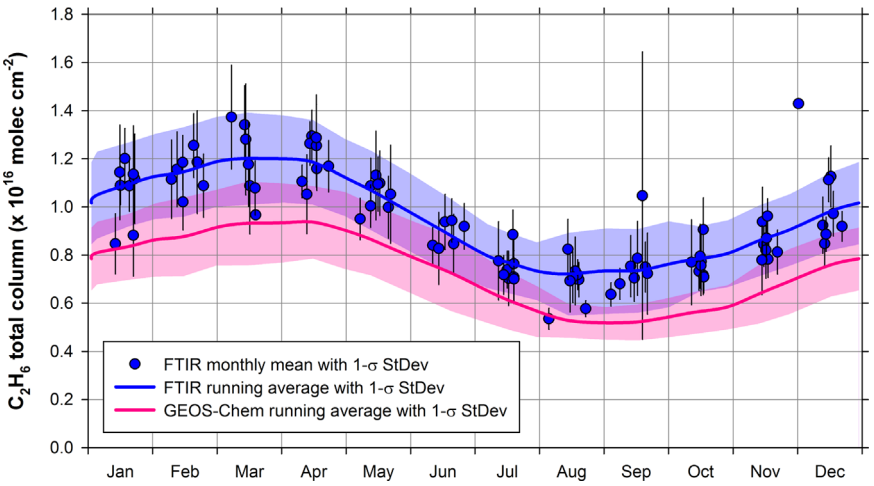


**Fig. 4.** Monthly-averaged total columns of $C_2H_6$ and associated 1-$\sigma$ standard deviation bars displayed on a 1-year time base, from the FTIR retrievals performed above ISSJ between July 2005 and May 2013. The blue curve and shaded area show on a 1-year time base the running mean fit to the daily-averaged columns (with a 2-month wide integration time and a 15-day time step) and the associated 1-$\sigma$ standard deviation, respectively. The red line and shaded area represent corresponding information, but deduced from the smoothed GEOS-Chem output. Note that the 1-$\sigma$ standard deviations around the running mean are calculated on the basis of the daily-averaged columns and hence include interannual fluctuations as well as variability of the monthly mean. (For interpretation of the references to color in this figure caption, the reader is referred to the web version of this paper.)

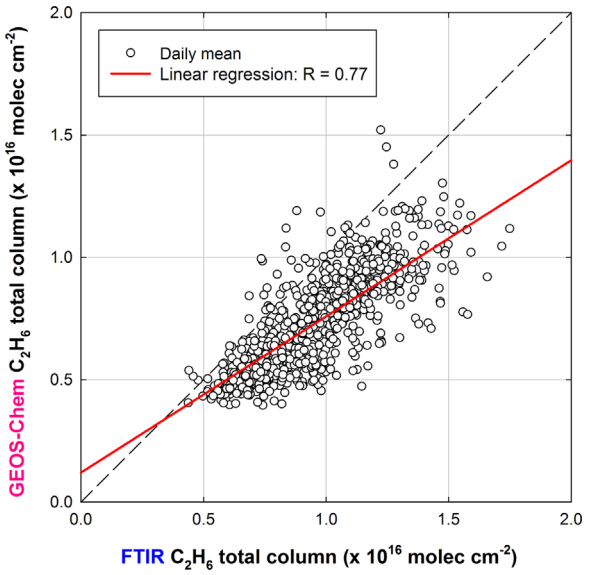


**Fig. 5.** FTIR daily-averaged total columns of $C_2H_6$ versus daily-averaged $C_2H_6$ abundances derived from smoothed GEOS-Chem profiles over the July 2005–May 2013 time span. The straight red line corresponds to the linear regression (with *R* as the correlation coefficient) between both data sets. (For interpretation of the references to color in this figure caption, the reader is referred to the web version of this paper.)

the $C_2H_6$ emissions used by the model that were developed only considering data collected prior to 2004. Incorporating updated and more accurate emission inventories into GEOS-Chem is the focus of ongoing work and is beyond the scope of this paper.

The retrieved columns of $C_2H_6$ at ISSJ are consistent with ground-based FTIR measurements from other stations in terms of amounts and seasonal cycle, taking into account the latitude and elevation of the ISSJ station (see [5,20–25,67]). At high-altitude stations such as ISSJ, lower burden and seasonal amplitude are generally observed due to high concentrations of $C_2H_6$ in the lowest tropospheric layers [23]. For instance, monthly-mean columns ranging between $1.76 \pm 0.40$ and $3.36 \pm 0.30 \times 10^{16}$ molec $cm^{-2}$ and a corresponding seasonal amplitude of 63% were obtained from ground-based FTIR solar spectra recorded over 1995–2000 at two Northern Hemisphere mid-latitude (44°N) stations located almost at the sea level in Japan [21]. The amplitude of the seasonal cycle is generally larger at high-latitude sites because of the enhanced fossil fuel emissions [67] and very weak oxidation rate by OH radicals in winter, allowing $C_2H_6$ to accumulate substantially during this season. At Eureka, [25] retrieved monthly-mean $C_2H_6$ columns between 1.2 and $2.85 \times 10^{16}$ molec $cm^{-2}$ from FTIR observations for 2007–2011, and the amplitude of the seasonal cycle was 93%.

### 5.2. Long-term trend

Fig. 6 presents the long-term time series of daily-averaged $C_2H_6$ total columns (in molec $cm^{-2}$) retrieved from the ISSJ solar spectra for the September 1994–August 2014 time period, which consists of 11,859 measurements spread over 2224 days of observation. The error bars associated with these daily means correspond to the 1-$\sigma$ standard deviation of the measurements within each day. This FTIR database homogeneously covers the investigated time span. We have used the statistical bootstrap resampling tool developed as in [22] to fit the whole daily time series in order to determine the $C_2H_6$ long-term linear trend (as well as the associated uncertainty) and the seasonal modulation. This bootstrap method combines a linear function and a 3rd order Fourier series taking into account the intra-annual variability of the data set.

Moreover, a running mean of the daily average data with a 3-year wide integration time and a 6-month step has revealed a minimum in the time series between the end of 2008 and the beginning of 2009. Therefore we have fitted both 1994–2008 and 2009–2014 time periods separately with the bootstrap tool that has returned two statistically-significant trends of $C_2H_6$ total columns at the 2-$\sigma$ confidence level: $-9.56 \pm 1.91 \times 10^{13}$ molec $cm^{-2}$ $year^{-1}$ and $4.35 \pm 0.81 \times 10^{14}$ molec $cm^{-2}$ $year^{-1}$, respectively. Then we have used both 1995.0 and 2009.0 columns modeled by the bootstrap tool as references in order to calculate the relative annual trends.

Analysis of the 1994–2008 time span reveals a regular decrease of the $C_2H_6$ amounts above ISSJ by $-0.92 \pm 0.18\%$ $year^{-1}$ relative to 1995.0. This negative trend is consistent with measurements and corresponding trends of atmospheric $C_2H_6$ burden presented in [66,68], both studies attributed the decline of global $C_2H_6$ emissions from the mid-1980s to reduced fugitive emissions from fossil fuel sources in Northern Hemisphere rather than a decrease in biomass burning and biofuel use (the other major sources of $C_2H_6$). These fugitive emissions mainly include natural gas loss due to evaporation, venting and flaring as well as equipment leaks during the production and processing of natural gas and oil. Consistent trends derived from FTIR solar spectra have already been reported at ISSJ by previous studies, but over shorter time periods: $-2.70 \pm 0.30\%$ $year^{-1}$ over 1985–1995 [27], $-1.20 \pm 0.65\%$ $year^{-1}$ over 1995–1999 [19], $-1.05 \pm 0.35\%$ $year^{-1}$ over 1995–2004 [22] and $-1.51 \pm 0.23\%$ $year^{-1}$ over 1996–2006 [23]. Global $C_2H_6$ emissions did not decline as rapidly between 2000 and 2010 period compared to the 1980s and 1990s [66,68], and this is consistent with our reported negative trend, which is smaller than reported in previous ISSJ studies.

Conversely, for the 2009–2014 time period, the bootstrap tool reveals a strong positive trend of $C_2H_6$ total columns of $4.90 \pm 0.91\%$ $year^{-1}$ relative to 2009.0 above ISSJ. We have also applied the bootstrap tool to the 3.58–8.88 and 8.88–22.10 km partial columns of $C_2H_6$ above ISSJ (see Section 3.1) and have found very similar positive trends relative to 2009.0, suggesting a vertically-homogeneous increase of $C_2H_6$ throughout the troposphere (and lower stratosphere). To our knowledge, this recent increase of the $C_2H_6$ burden in the background atmosphere has not been reported and its origin is still unidentified.

A hypothetical source may be enhanced fugitive emissions of $C_2H_6$ linked to the recent growth in the exploitation of shale gas and tight oil reservoirs. The growth has been especially massive in North America. Indeed, positive

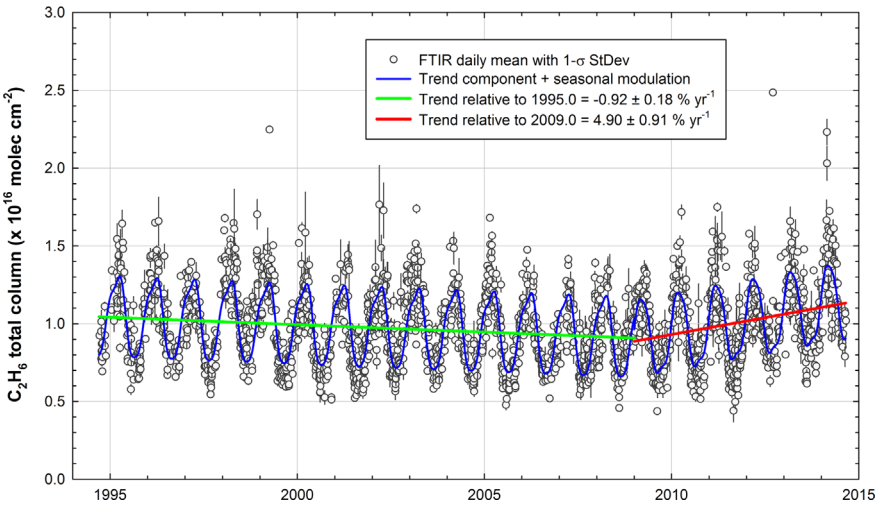


**Fig. 6.** FTIR time series of daily-averaged $C_2H_6$ total columns and associated 1-$\sigma$ standard deviation bars above ISSJ from September 1994 to August 2014. The functions fitted to all available daily means (including seasonal modulation and trend component) and calculated by the bootstrap resampling tool of [22] over the 1994–2008 and 2009–2014 time periods are drawn in blue curve. The green and red solid lines correspond to the trend components of these fitting functions. (For interpretation of the references to color in this figure caption, the reader is referred to the web version of this paper.)

anomalies of $CH_4$ related to the oil and gas industries have been recently detected from space over regions of North America where the drilling productivity began to grow rapidly after 2009 (see [69]). This hypothesis is supported by measurements derived from 1986 solar occultation observations performed over North America (16°–88°N and 173°–50°W) between 2004 and the middle of 2013 by the ACE-FTS instrument [70]. We employed the version 3.5 ACE-FTS data [71], which includes an improved retrieval strategy for $C_2H_6$, within the 8–16 km altitude range. Applying the bootstrap tool to the ACE-FTS partial columns over the 2004–2008 and 2009–2013 time periods, we have calculated statistically-significant trends (at the 2-$\sigma$ level) of $-1.75 \pm 1.30$ and $9.4 \pm 3.2\%\ \text{year}^{-1}$ relative to 2004.0 and 2009.0, respectively, which are consistent with the FTIR trends when accounting for the associated uncertainty ranges. Trends derived from 906 ACE-FTS measurements between 10° and 40°S do not reveal any recent increase of the $C_2H_6$ burden. Instead these data show a statistically significant decrease ($-1.62 \pm 1.08\%\ \text{year}^{-1}$) over the 2004 to mid-2013 time period. This suggests that the observed increase of $C_2H_6$ is limited to the Northern Hemisphere.

It is worth noting that the GEOS-Chem CTM does not reproduce this recent increase in the abundance of $C_2H_6$ above ISSJ, suggesting emission inventories for $C_2H_6$ and other light alkanes may not be properly accounting for the enhanced fugitive emissions from recent natural gas and oil production.

## 6. Discussions and conclusions

In this study, we have developed and optimized a new strategy based on an improved spectroscopy to retrieve $C_2H_6$ total and partial columns from ground-based FTIR solar spectra recorded at the dry and high-altitude ISSJ. The selected spectroscopic parameters accounted for in the three micro-windows include $C_2H_6$ pseudo-lines based on cross-section laboratory spectra as well as updated line features for $O_3$ and $CH_3Cl$. Such an improved spectroscopy has yielded substantially reduced fitting residuals, enhanced information content (with a mean DOFS of $2.11 \pm 0.27$ for the whole data set) and less solar spectra discarded because of ungeophysical mixing ratio profiles.

We have applied this strategy to the long-term FTIR time series available at ISSJ (spanning 1994–2014) and compared the retrieved total columns to $C_2H_6$ columns simulated by the GEOS-Chem CTM, taking into account the vertical sensitivity of the retrievals by convolving the modeled profiles with the FTIR averaging kernels. The observations and the model present consistent seasonal cycles, but GEOS-Chem under-predicts the observed $C_2H_6$ burden throughout the seasonal cycle. This suggests an underestimation of $C_2H_6$ emissions in the model and points to the need for improved inventories for further GEOS-Chem simulations and sensitivity tests.

Finally, we have presented the 20-year ISSJ time series of $C_2H_6$ column abundance. Using a bootstrap resampling tool, we have calculated a statistically-significant negative trend in $C_2H_6$ total columns until 2009, consistent with prior studies and with our understanding of global $C_2H_6$ emissions. However, the ISSJ time series has also revealed a strong positive trend in $C_2H_6$ over the last 6 years of the record, from 2009 onwards. Such a recent increase in the remote atmosphere is still unreported and, because of the involvement of $C_2H_6$ in the global VOC–$HO_x$–$NO_x$ chemistry responsible for generating or destroying tropospheric $O_3$, investigating both its cause and its impact on air quality should be a high priority for the atmospheric chemistry community.

This $C_2H_6$ increase extends beyond previous positive short-term anomalies already observed in the Northern Hemisphere, which occur every 3–5 years and are generally associated with variability in biomass burning emissions [66,72]. The seasonal cycle of $C_2H_6$ above ISSJ is primarily driven by the photochemical cycle of its main

sink (OH radicals). We argue that it is unlikely that the recent increase can be attributed to sharp fluctuations of OH concentration in the atmosphere because the global OH levels have not exhibited large interannual variability since the end of the 20th century [73]. Indeed, neither CO nor other species that have oxidation by OH as their major removal pathway such as hydrogen cyanide (HCN) and acetylene ($C_2H_2$), do not present an upturn in their retrieved columns above ISSJ over the last years. However, $CH_4$, which is closely linked to $C_2H_6$ [66,72], has also presented globally a renewed rise after 2006 [74]. We hypothesize that the observed recent increase in $C_2H_6$ above ISSJ could represent a change in $C_2H_6$ throughout the Northern Hemisphere and may be the product of a large increase in fugitive emissions related to the recent upturn in the development of North American shale gas and tight oil reservoirs.

The lifetime of $C_2H_6$ is approximately 2 months, and this makes $C_2H_6$ influenced by vertical mixing and long-range transport. Ethane is therefore a convenient tracer of anthropogenic activity for remote sensing [65]. Measurements of $C_2H_6$ in the remote troposphere can also be used to identify air masses that have originated in regions with significant oil and gas production [66]. Air masses impacted by intense episodes of biomass burning have already been detected in the retrieved $C_2H_6$ columns at ISSJ, associated with severe tropical emissions from Asia during the strong El Niño event of 1997–1998 [19]. Our future work will focus on combining an analysis of $C_2H_6$ measurements from ground-based FTIR solar spectra and observations from ACE-FTS with dedicated GEOS-Chem simulations with updated inventories. The goal will be to identify the cause of the recent increase in $C_2H_6$ and evaluate the magnitude of emissions required to produce the observed changes.

## Acknowledgments

The University of Liège contribution to the present work has mainly been supported by the AGACC-II project of the Science for Sustainable Development (SSD) program of the Belgian Science Policy Office (BELSPO, Brussels). Additional support was provided by MeteoSwiss (Global Atmospheric Watch), the Fédération Wallonie–Bruxelles and the F.R.S. – FNRS. We thank the International Foundation High Altitude Research Stations Jungfraujoch and Gornergrat (HFSJG, Bern). E. Mahieu is Research Associate with F.R.S. – FNRS. We are grateful to the many colleagues who have contributed to FTIR data acquisition at the Jungfraujoch station. We thank Jeremy Harrison and colleagues for their high quality lab measurements of $C_2H_6$. Part of this work was performed at the Jet Propulsion Laboratory, California Institute of Technology, under contract with NASA. Agnès Perrin would like to thank for financial support the French program LEFE-CHAT (Les Enveloppes Fluides et l'Environnement – Chimie Atmosphérique) of INSU (Institut des Sciences de l'Univers) from CNRS. Funding for Emily V. Fischer was provided by the U.S. National Oceanographic and Atmospheric Administration through award number NA14OAR4310148. This research was partly supported by the Global Environment Research Fund (S-7/12) by the Ministry of the Environment (MOE), Japan, and the Research Program on Climate Change Adaptation (RECCA) by the Ministry of Education, Culture, Sports, Science and Technology (MEXT), Japan. Funding for the Atmospheric Chemistry Experiment comes from the Canadian Space Agency.

## References

[1] Rudolph J. The tropospheric distribution and budget of ethane. J Geophys Res 1995;100(D6):11369–81. http://dx.doi.org/10.1029/95JD00693.

[2] Logan JA, Prather MJ, Wofsy SC, McElroy MB. Tropospheric chemistry: a global perspective. J Geophys Res 1981;86(C8):7210–54, http://dx.doi.org/10.1029/JC086iC08p07210.

[3] Xiao Y, Logan JA, Jacob DJ, Hudman RC, Yantosca R, Blake DR. Global budget of ethane and regional constraints on US sources. J Geophys Res 2008;113(D21306). http://dx.doi.org/10.1029/2007JD009415.

[4] Aikin AC, Herman JR, Maier EJ, McQuillan CJ. Atmospheric chemistry of ethane and ethylene. J Geophys Res 1982;87(C4):3105–18, http://dx.doi.org/10.1029/JC087iC04p03105.

[5] Rinsland CP. Multiyear infrared solar spectroscopic measurements of HCN, CO, $C_2H_6$, and $C_2H_2$ tropospheric columns above Lauder, New Zealand (45°S latitude). J Geophys Res 2002;107(D14). http://dx.doi.org/10.1029/2001JD001150.

[6] Collins WJ, Derwent RG, Johnson CE, Stevenson DS. The oxidation of organic compounds in the troposphere and their global warming potentials. Clim Change 2002;52:453–79. http://dx.doi.org/10.1023/A:1014221225434.

[7] Fischer EV, Jacob DJ, Yantosca RM, Sulprizio MP, Millet DB, Mao J, et al. Atmospheric peroxyacetyl nitrate (PAN): a global budget and source attribution. Atmos Chem Phys 2014;14:2679–98, http://dx.doi.org/10.5194/acp-14-2679-2014.

[8] Toon GC. The JPL MkIV interferometer. Optics Photonics News 1991;2(10):19–21. http://dx.doi.org/10.1364/OPN.2.10.000019.

[9] Blake DR, Chen TY, Smith Jr. TW, Wang CJL, Wingenter OW, Blake NJ, et al. Three-dimensional distribution of nonmethane hydrocarbons and halocarbons over the northwestern Pacific during the 1991 Pacific Exploratory Mission (PEM-West A). J Geophys Res 1996;101(D1):1763–78. http://dx.doi.org/10.1029/95JD02707.

[10] Fishman J, Hoell JM, Bendura RD, McNeal RJ, Kirchhoff VWJH. NASA GTE TRACE A experiment (September–October 1992): overview. J Geophys Res 1996;101(D19):23865–79. http://dx.doi.org/10.1029/96JD00123.

[11] Chatfield RB, Vastano JA, Li L, Sachse GW, Connors VS. The Great African Plume from biomass burning: generalizations from a three-dimensional study of TRACE A carbon monoxide. J Geophys Res 1998;103(D21):28059–77. http://dx.doi.org/10.1029/97JD03363.

[12] Rinsland CP, Dufour G, Boone CD, Bernath PF, Chiou L. Atmospheric Chemistry Experiment (ACE) measurements of elevated Southern Hemisphere upper tropospheric CO, $C_2H_6$, HCN, and $C_2H_2$ mixing ratios from biomass burning emissions and long-range transport. Geophys Res Lett 2005;32(20). http://dx.doi.org/10.1029/2005GL024214.

[13] Browell EV, Hair JW, Butler CF, Grant WB, DeYoung RJ, et al. Ozone, aerosol, potential vorticity, and trace gas trends observed at high-latitudes over North America from February to May 2000. J Geophys Res 2003;108(D4):8369. http://dx.doi.org/10.1029/2001JD001390.

[14] Swanson AL, Blake NJ, Atlas E, Flocke F, Blake DR, Rowland FS. Seasonal variations of $C_2$–$C_4$ nonmethane hydrocarbons and $C_1$–$C_4$ alkyl nitrates at the Summit research station in Greenland. J Geophys Res 2003;108(D2):4064. http://dx.doi.org/10.1029/2001JD001445.

[15] Wingenter OW, Sive BC, Blake NJ, Blake DR, Rowland FS. Atomic chlorine concentrations derived from ethane and hydroxyl measurements over the equatorial Pacific Ocean: implication for dimethyl sulfide and bromine monoxide. J Geophys Res 2005;110(D20308). http://dx.doi.org/10.1029/2005JD005875.

[16] Glatthor N, von Clarmann T, Stiller GP, Funke B, Koukouli ME, Fischer H, et al. Large-scale upper tropospheric pollution observed by MIPAS HCN and $C_2H_6$ global distributions. Atmos Chem Phys 2009;9:9619–34. http://dx.doi.org/10.5194/acp-9-9619-2009.

[17] Rinsland CP, Jones NB, Connor BJ, Logan JA, Pougatchev NS, Goldman A, et al. Northern and southern hemisphere ground-based infrared spectroscopic measurements of tropospheric carbon monoxide and

ethane. J Geophys Res 1998;103(D21):28197–217. http://dx.doi.org/10.1029/98JD02515.
[18] Rinsland CP, Goldman A, Murcray FJ, Stephen TM, Pougatchev NS, Fishman J, et al. Infrared solar spectroscopic measurements of free tropospheric CO, $C_2H_6$, and HCN above Mauna Loa, Hawaii: seasonal variations and evidence for enhanced emissions from the Southeast Asian tropical fires of 1997–1998. J Geophys Res 1999;104(D15): 18667–80. http://dx.doi.org/10.1029/1999JD900366.
[19] Rinsland CP, Mahieu E, Zander R, Demoulin P, Forrer J, Buchmann B. Free tropospheric CO, $C_2H_6$, and HCN above central Europe: recent measurements from the Jungfraujoch station including the detection of elevated columns during 1998. J Geophys Res 2000;105(D19): 24235–49. http://dx.doi.org/10.1029/2000JD900371.
[20] Rinsland CP, Meier A, Griffith DWT, Chiou LS. Ground-based measurements of tropospheric CO, $C_2H_6$, and HCN from Australia at 34°S latitude during 1997–1998. J Geophys Res 2001;106(D18): 20913–24. http://dx.doi.org/10.1029/2000JD000318.
[21] Zhao Y, Strong K, Kondo Y, Koike M, Matsumi Y, Irie H, et al. Spectroscopic measurements of tropospheric CO, $C_2H_6$, $C_2H_2$, and HCN in northern Japan. J Geophys Res 2002;107(D18):4343, http://dx.doi.org/10.1029/2001JD000748.
[22] Gardiner T, Forbes A, de Mazière M, Vigouroux C, Mahieu E, Demoulin P, et al. Trend analysis of greenhouse gases over Europe measured by a network of ground-based remote FTIR instruments. Atmos Chem Phys 2008;86719–27. doi:http://dx.doi.org/10.5194/acp-8-6719-2008.
[23] Angelbratt J, Mellqvist J, Simpson D, Jonso JE, Blumenstock T, Borsdorff T, et al. Carbon monoxide (CO) and ethane ($C_2H_6$) trends from ground-based solar FTIR measurements at six European stations, comparison and sensitivity analysis with the EMEP model. Atmos Chem Phys 2011;11:9253–69. http://dx.doi.org/10.5194/acp-11-9253-2011.
[24] Vigouroux C, Stavrakou T, Whaley C, Dils B, Duflot V, Hermans C, et al. FTIR time-series of biomass burning products (HCN, $C_2H_6$, $C_2H_2$, $CH_3OH$, and HCOOH) at Reunion Island (21°S, 55°E) and comparisons with model data. Atmos Chem Phys 2012;12: 10367–85. http://dx.doi.org/10.5194/acp-12-10367-2012.
[25] Viatte C, Strong K, Walker KA, Drummond JR. Five years of CO, HCN, $C_2H_6$, $C_2H_2$, $CH_3OH$, HCOOH and $H_2CO$ total columns measured in the Canadian high Arctic. Atmos Meas Tech 2014;7:1547–70, http://dx.doi.org/10.5194/amt-7-1547-2014.
[26] Zander R, Mahieu E, Demoulin P, Duchatelet P, Roland G, Servais C, et al. Our changing atmosphere: evidence based on long-term infrared solar observations at the Jungfraujoch since 1950. Sci Total Environ 2008;391 (2–3):184–95. http://dx.doi.org/10.1016/j.scitotenv.2007.10.018.
[27] Mahieu E, Zander R, Delbouille L, Demoulin P, Roland G, Servais C. Observed trends in total vertical column abundances of atmospheric gases from IR solar spectra recorded at the Jungfraujoch. J Atmos Chem 1997;28:227–43. http://dx.doi.org/10.1023/A:1005854-926740.
[28] Zellweger C, Forrer J, Hofer P, Nyeki S, Schwarzenbach B, Weingartner E, et al. Partitioning of reactive nitrogen ($NO_y$) and dependence on meteorological conditions in the lower free troposphere. Atmos Chem Phys 2003;3:779–96. http://dx.doi.org/10.5194/acp-3-779-2003.
[29] Reimann S, Schaub D, Stemmler K, Folini D, Hill M, Hofer P, et al. Halogenated greenhouse gases at the Swiss High Alpine Site of Jungfraujoch (3580 m asl): continuous measurements and their use for regional European source allocation. J Geophys Res 2004;109 (D05307). http://dx.doi.org/10.1029/2003JD003923.
[30] Rodgers CD. Characterization and error analysis of profiles retrieved from remote sounding measurements. J Geophys Res 1990;95(D5): 5587–95. http://dx.doi.org/10.1029/JD095iD05p05587.
[31] Drayson SR. Rapid computation of the Voigt profile. J Quant Spectrosc Radiat Transf 1976;16:611–4. http://dx.doi.org/10.1016/0022-4073(76)90029-7.
[32] Pine AS, Rinsland CP. The role of torsional hot bands in modeling atmospheric ethane. J Quant Spectrosc Radiat Transf 1999;62: 445–58. http://dx.doi.org/10.1016/S0022-4073(98)00114-9.
[33] Paton-Walsh C, Deutscher NM, Griffith DWT, Forgan BW, Wilson SR, Jones NB, Edwards DP. Trace gas emissions from savanna fires in northern Australia. J Geophys Res 2010;115(D16314). http://dx.doi.org/10.1029/2009JD013309.
[34] Meier A, Toon GC, Rinsland CP, Goldman A, Hase F. spectroscopic atlas of atmospheric microwindows in the middle infra-red. Kiruna, Sweden: IRF Institutet för Rymdfysik; 2004.
[35] Notholt J, Toon GC, Lehmann R, Sen B, Blavier J-F. Comparison of Arctic and Antarctic trace gas column abundances from ground-based Fourier transform infrared spectrometry. J Geophys Res 1997;102(D11):12863–9. http://dx.doi.org/10.1029/97JD00358.
[36] Hase F, Demoulin P, Sauval AJ, Toon GC, Bernath PF, Goldman A, et al. An empirical line-by-line model for the infrared solar transmittance spectrum from 700 to 5000 $cm^{-1}$. J Quant Spectrosc Radiat Transf 2006;102:450–63. http://dx.doi.org/10.1016/j.jqsrt.2006.02.026.
[37] Sudo K, Takahashi M, Kurokawa J, Akimoto H. Chaser: a global chemical model of the troposphere, 1. Model description. J Geophys Res 2002;107(D17):4339. http://dx.doi.org/10.1029/2001JD001113.
[38] Chang L, Palo S, Hagan M, Richter J, Garcia R, Riggin D, Fritts D. Structure of the migrating diurnal tide in the Whole Atmosphere Community Climate Model (WACCM). Adv Space Res 2008;41: 1398–407. http://dx.doi.org/10.1016/j.asr.2007.03.035.
[39] Rodgers CD, Connor BJ. Intercomparison of remote sounding instruments. J Geophys Res 2003;108(D3):4116. http://dx.doi.org/10.1029/2002JD002299.
[40] Pine AS, Lafferty WJ. Torsional splittings and assignments of the Doppler-limited spectrum of ethane in the CH stretching region. J Res Natl Bur Stand 1981;87(3):237–56.
[41] Brown LR, Farmer CB, Rinsland CP, Toth RA. Molecular line parameters for the atmospheric trace molecule spectroscopy experiment. Appl Opt 1987;26(23):5154–82.
[42] Rothman LS, et al. The HITRAN 2004 molecular spectroscopic database. J Quant Spectrosc Radiat Transf 2005;96:139–204, http://dx.doi.org/10.1016/j.jqsrt.2004.10.008.
[43] Rothman LS, et al. The HITRAN 2008 molecular spectroscopic database. J Quant Spectrosc Radiat Transf 2009;110:533–72, http://dx.doi.org/10.1016/j.jqsrt.2009.02.013.
[44] Harrison JJ, Allen NDC, Bernath PF. Infrared absorption cross sections for ethane ($C_2H_6$) in the 3 μm region. J Quant Spectrosc Radiat Transf 2010;111:357–63. http://dx.doi.org/10.1016/j.jqsrt.2009.09.010.
[45] Lattanzi F, di Lauro C, Vander Auwera F. Toward the understanding of the high resolution infrared spectrum of $C_2H_6$ near 3.3 μm. J Mol Spec 2011;267(1–2):71–9. http://dx.doi.org/10.1016/j.jms.2011.02.003.
[46] Rothman LS, et al. The HITRAN 2012 molecular spectroscopic database. J Quant Spectrosc Radiat Transf 2013;130:4–50, http://dx.doi.org/10.1016/j.jqsrt.2013.07.002.
[47] Bray C, Perrin A, Jacquemart D, Lacome N. The $\nu_1$, $\nu_4$ and $3\nu_6$ bands of methyl chloride in the 3.4−μm region: line positions and intensities. J Quant Spectrosc Radiat Transf 2011;112:2446–62. http://dx.doi.org/10.1016/j.jqsrt.2011.06.018.
[48] Bray C, Jacquemart D, Buldyreva J, Lacome N, Perrin A. $N_2$-broadening coefficients of methyl chloride at room temperature. J Quant Spectrosc Radiat Transf 2012;113:1102–12. http://dx.doi.org/10.1016/j.jqsrt.2012.01.028.
[49] Esposito F, Grieco G, Masiello G, Pavese G, Restieri R, Serio C, Cuomo V. Intercomparison of line-parameter spectroscopic databases using downwelling spectral radiance. Q J R Meteorol Soc 2007;133:191–202. http://dx.doi.org/10.1002/qj.131.
[50] Rodgers C. Inverse methods for atmospheric sounding, vol. 2 of Series on Atmospheric, Oceanic and Planetary Physics 2000.
[51] Vigouroux C, Hendrick F, Stavrakou T, Dils B, De Smedt I, Hermans C, et al. Ground-based FTIR and MAX-DOAS observations of formaldehyde at Réunion Island and comparisons with satellite and model data. Atmos Chem Phys 2009;9:9523–44. http://dx.doi.org/10.5194/acp-9-9523-2009.
[52] Rinsland CP, Mahieu E, Demoulin P, Zander R, Servais C, Hartmann J-M. Decrease of the carbon tetrachloride ($CCl_4$) loading above Jungfraujoch, based on high resolution infrared solar spectra recorded between 1999 and 2011. J Quant Spectrosc Radiat Transf 2012;113:1322–9, http://dx.doi.org/10.1016/j.jqsrt.2012.02.016.
[53] Hase F, Hannigan JW, Coffey MT, Goldman A, Höpfner M, Jones NB, et al. Intercomparison of retrieval codes used for the analysis of high-resolution: ground-based FTIR measurements. J Quant Spectrosc Radiat Transf 2004;87:25–52. http://dx.doi.org/10.1016/j.jqsrt.2003.12.008.
[54] Franco B, Hendrick F, Van Roozendael M, Müller J-F, Stavrakou T, Marais EA, et al. Retrievals of formaldehyde from ground-based FTIR and MAX-DOAS observations at the Jungfraujoch station and comparisons with GEOS-Chem and IMAGES model simulations. Atmos Meas Tech Discuss 2014;7:10715–70. http://dx.doi.org/10.5194/amtd-7-10715-2014.
[55] Sudo K, Akimoto H. Global source attribution of tropospheric ozone: long-range transport from various source regions. J Geophys Res 2007;112(D12302). http://dx.doi.org/10.1029/2006JD007992.
[56] Takemura T, Nozawa T, Emori S, Nakajima TY, Nakajima T. Simulation of climate response to aerosol direct and indirect effects with aerosol transport-radiation model. J Geophys Res 2005;110 (D02202). http://dx.doi.org/10.1029/2004JD005029.

[57] Watanabe S, Hajima T, Sudo K, Nagashima T, Takemura T, Okajima H, et al. MIROC-ESM 2010: model description and basic results of CMIP5-20c3m experiments. Geosci Model Dev 2011;4:845–72, http://dx.doi.org/10.5194/gmd-4-845-2011.
[58] Ito A. Evaluation of the impacts of defoliation by tropical cyclones on a Japanese forest's carbon budget using flux data and a process-based model. J Geophys Res 2010;115(G04013). http://dx.doi.org/10.1029/2010JG001314.
[59] Bey I, Jacob DJ, Yantosca RM, Logan JA, Field BD, Fiore AM, et al. Global modeling of tropospheric chemistry with assimilated meteorology: model description and evaluation. J Geophys Res 2001;106(D19):23073–95. http://dx.doi.org/10.1029/2001JD000807.
[60] Park RJ, Jacob DJ, Field BD, Yantosca RM, Chin M. Natural and transboundary pollution influences on sulfate-nitrate-ammonium aerosols in the United States: implications for policy. J Geophys Res 2004;109(D15204). http://dx.doi.org/10.1029/2003JD004473.
[61] Mao J, Jacob DJ, Evans MJ, Olson JR, Ren X, Brune WH, et al. Chemistry of hydrogen oxide radicals ($HO_x$) in the Arctic troposphere in spring. Atmos Chem Phys 2010;10:5823–38. http://dx.doi.org/10.5194/acp-10-5823-2010.
[62] Van het Bolscher M, Pereira J, Spessa A, Dalsoren S, van Nojie T, Szopa S. REanalysis of the TROpospheric chemical composition over the past 40 years. Hamburg, Germany: Max Plank Institute for Meteorology; 2008.
[63] Van der Werf GR, Randerson JT, Giglio L, Collatz GJ, Mu M, Kasibhatla PS, et al. Global fire emissions and the contribution of deforestation, savanna, forest, agricultural, and peat fires 1997–2009. Atmos Chem Phys 2010;10:11707–35. http://dx.doi.org/10.5194/acp-10-11707-2010.
[64] Pozzer A, Pollmann J, Taraborrelli D, Jöckel P, Helmig D, Tans P, et al. Observed and simulated global distribution and budget of atmospheric $C_2$–$C_5$ alkanes. Atmos Chem Phys 2010;10:4403–22, http://dx.doi.org/10.5194/acp-10-4403-2010.
[65] Ehhalt DH, Schmidt U, Zander R, Demoulin P, Rinsland CP. Seasonal cycle and secular trend of the total and tropospheric column abundance of ethane above the Jungfraujoch. J Geophys Res 1991;96(D3):4985–94. http://dx.doi.org/10.1029/90JD02229.
[66] Simpson IJ, Sulbaek Andersen MP, Meinardi S, Bruhwiler L, Blake NJ, Helmig D, et al. Long-term decline of global atmospheric ethane concentrations and implications for methane. Nature 2012;488:490–4. http://dx.doi.org/10.1038/nature11342.
[67] Zeng G, Wood SW, Morgenstern O, Jones NB, Robinson J, Smale D. Trends and variations in CO, $C_2H_6$, and HCN in the Southern Hemisphere point to the declining anthropogenic emissions of CO and $C_2H_6$. Atmos Chem Phys 2012;12:7543–55. http://dx.doi.org/10.5194/acp-12-7543-2012.
[68] Aydin M, Verhulst KR, Saltzman ES, Battle MO, Montzka SA, Blake DR, et al. Recent decreases in fossil-fuel emissions of ethane and methane derived from firn air. Nature 2011;476:198–201, http://dx.doi.org/10.1038/nature10352.
[69] Schneising O, Burrows JP, Dickerson RR, Buchwitz M, Reuter M, Bovensmann H. Remote sensing of fugitive methane emissions from oil and gas production in North American tight geologic formations: remote sensing of fugitive methane emissions from oil and gas production. Earth's Future 2014;2:548–58. http://dx.doi.org/10.1002/2014EF000265.
[70] Bernath PF, McElroy CT, Abrams MC, Boone CD, Butler M, et al. Atmospheric chemistry experiment ACE: mission overview. Geophys Res Lett 2005;32(L15S01). http://dx.doi.org/10.1029/2005GL022386.
[71] Boone CD, Walker KA, Bernath PF. Version 3 retrievals for the atmospheric chemistry experiment fourier transform spectrometer (ACE-FTS), The atmospheric chemistry experiment ACE at 10: a solar occultation anthology. Hampton, Virginia: A. Deepak Publishing; 2013.
[72] Simpson IJ, Rowland FS, Meinardi S, Blake DR. Influence of biomass burning during recent fluctuations in the slow growth of global tropospheric methane. Geophys Res Lett 2006;33(L22808). http://dx.doi.org/10.1029/2006GL027330.
[73] Montzka SA, Krol M, Dlugokencky E, Hall B, Jockel P, Lelieveld J. Small interannual variability of global atmospheric hydroxyl. Science 2011;331:67–9. http://dx.doi.org/10.1126/science.1197640.
[74] Kirschke S, Bousquet P, Ciais P, Saunois M, Canadell JG, et al. Three decades of global methane sources and sinks. Nat Geosci 2013;6:813–23. http://dx.doi.org/10.1038/ngeo1955.